



# Global silicate weathering flux overestimated because of sediment–water cation exchange

Edward T. Tipper<sup>a,1</sup> ID, Emily I. Stevenson<sup>a</sup>, Victoria Alcock<sup>a</sup> ID, Alasdair C. G. Knight<sup>a</sup> ID, J. Jotautas Baronas<sup>a</sup> ID, Robert G. Hilton<sup>b</sup>, Mike J. Bickle<sup>a</sup> ID, Christina S. Larkin<sup>a</sup> ID, Linshu Feng<sup>a</sup>, Katy E. Relph<sup>a</sup>, and Genevieve Hughes<sup>a</sup>

<sup>a</sup>Department of Earth Sciences, University of Cambridge, Cambridge CB2 3EQ, United Kingdom; and <sup>b</sup>Department of Geography, Durham University, Durham DH1 3LE, United Kingdom

Edited by Andrea Rinaldo, École Polytechnique Fédérale de Lausanne, Lausanne, Switzerland, and approved November 18, 2020 (received for review August 4, 2020)

Rivers carry the dissolved and solid products of silicate mineral weathering, a process that removes CO<sub>2</sub> from the atmosphere and provides a key negative climate feedback over geological timescales. Here we show that, in some river systems, a reactive exchange pool on river suspended particulate matter, bonded weakly to mineral surfaces, increases the mobile cation flux by 50%. The chemistry of both river waters and the exchange pool demonstrates exchange equilibrium, confirmed by Sr isotopes. Global silicate weathering fluxes are calculated based on riverine dissolved sodium (Na<sup>+</sup>) from silicate minerals. The large exchange pool supplies Na<sup>+</sup> of nonsilicate origin to the dissolved load, especially in catchments with widespread marine sediments, or where rocks have equilibrated with saline basement fluids. We quantify this by comparing the riverine sediment exchange pool and river water chemistry. In some basins, cation exchange could account for the majority of sodium in the river water, significantly reducing estimates of silicate weathering. At a global scale, we demonstrate that silicate weathering fluxes are overestimated by 12 to 28%. This overestimation is greatest in regions of high erosion and high sediment loads where the negative climate feedback has a maximum sensitivity to chemical weathering reactions. In the context of other recent findings that reduce the net CO<sub>2</sub> consumption through chemical weathering, the magnitude of the continental silicate weathering fluxes and its implications for solid Earth CO<sub>2</sub> degassing fluxes need to be further investigated.

cation exchange | global biogeochemical cycles | suspended particulate matter | silicate weathering

For decades, silicate weathering has been postulated to provide the negative climate feedback on Earth that prevents a runaway greenhouse climate like on Venus (1). Silicate mineral dissolution with carbonic acid converts atmospheric CO<sub>2</sub> into carbonate, and releases essential nutrients to the terrestrial and marine biosphere (2). There have been many attempts to quantify the silicate weathering flux (3), mostly assuming that riverine dissolved sodium (Na<sup>+</sup>) is derived only from silicate minerals and rock salt. Here we show that there is a major addition of nonsilicate Na<sup>+</sup> to the critical zone from ancient seawater, weakly bonded to sedimentary rocks and supplied to waters via the cation exchange process. The implication is not only that the silicate weathering flux is overestimated at a global scale, but that this nonsilicate Na<sup>+</sup> is most important in regions previously thought to have the highest silicate weathering fluxes (so called weathering-limited regions) and greatest climate sensitivity.

Cation exchange is a rapid chemical reaction between cations in the dissolved phase and mineral surfaces, particularly clays (4). Major and trace cations such as calcium (Ca<sup>2+</sup>), magnesium (Mg<sup>2+</sup>), sodium (Na<sup>+</sup>), potassium (K<sup>+</sup>), and strontium (Sr<sup>2+</sup>) form the cation exchange pool, which balances negative charges on river-borne clay particle surfaces. This exchange takes place on interlayer sites, between the tetrahedral and octahe-

dral layers, or on exposed surfaces (4). The importance of the cation exchange pool is well recognized in soils and aquifers (4, 5), has significant implications for enhanced weathering (6), and has been proposed as an important mechanism for buffering the composition of river waters (7–9). However, data on the riverine exchange pool are only available for two large river systems [Amazon and Ganges-Brahmaputra (10, 11)], despite its significance in providing a source of elements that are immediately bioavailable (12), and their potential for biasing the quantification of silicate weathering (9).

It is increasingly recognized that rapidly reactive phases have a strong influence on the chemistry of river waters (13, 14). Cation exchange is a rapid reaction occurring continuously in soils, as riverine freshwaters evolve downstream interacting with particulate matter, and when they mix with seawater (15, 16). Important examples of cation exchange are the “swapping” of divalent cations Ca<sup>2+</sup> and Mg<sup>2+</sup> with Na<sup>+</sup>, in particular when there is a major change in water composition such as when fluvial clays reach the ocean,



As a result, marine sediments have an exchange pool that is dominated by Na<sup>+</sup> (17). Subsequently, these marine sediments are uplifted and emplaced on the continents where Na<sup>+</sup> in the exchange pool is released by cation exchange with Ca-rich fresh waters (9). This has major implications for estimates of silicate weathering fluxes and associated CO<sub>2</sub> consumption,

## Significance

Large rivers transport water and sediment to floodplains and oceans, supplying the nutrients that sustain life. They also transport carbon, removed from the atmosphere during mineral dissolution reactions, which is thought to provide a key negative climate feedback on long timescales. We demonstrate that the (million-year) carbon flux associated with mineral dissolution has been overestimated by up to 28% because of a reactive pool of elements transported with river-borne suspended sediment. This is most acute in regions of high erosion, where silicate weathering is thought to be most intense.

Author contributions: E.T.T. designed research; E.T.T., E.I.S., V.A., A.C.G.K., and J.J.B. performed research; E.T.T., E.I.S., V.A., A.C.G.K., J.J.B., C.S.L., L.F., K.E.R., and G.H. analyzed data; and E.T.T., E.I.S., V.A., A.C.G.K., J.J.B., R.G.H., M.J.B., C.S.L., and K.E.R. wrote the paper.

The authors declare no competing interest.

This article is a PNAS Direct Submission.

Published under the PNAS license.

<sup>1</sup>To whom correspondence may be addressed. Email: ett20@cam.ac.uk.

This article contains supporting information online at <https://www.pnas.org/lookup/suppl/doi:10.1073/pnas.2016430118/DCSupplemental>.

Published December 21, 2020.

because they are calculated using the  $\text{Na}^+$  content of rivers (3). Cerling et al. (9) proposed that the  $\text{Na}^+$ -rich exchange pool exerts an important control on natural waters, based on charge balance arguments from river water chemistry, but this hypothesis has never been rigorously tested (18) by determining the flux and composition of the exchange pool of rivers around the world.

In this contribution, we present a large dataset of fluvial sediment cation exchange capacity (CEC) and composition in several of the world's largest river basins. By comparing with the concomitant dissolved load chemistry, we demonstrate that 1) the exchange pool in river sediments is in equilibrium with the river water; 2) the fraction of mobile elements in the exchange pool relative to the dissolved pool can be significant, particularly in rapidly eroding, weathering-limited catchments; and 3) given reasonable inferences on the composition of old marine sedimentary rocks, modern-day silicate weathering has been overestimated and carbonate weathering has been underestimated. The results reduce the estimated magnitude of the silicate weathering flux, but increase the supply of base cations (e.g.,  $\text{Ca}^{2+}$ , which can be a limiting nutrient) to the biosphere, suggesting a greater role of organic carbon burial compared with silicate weathering for the long-term atmospheric  $\text{CO}_2$  sink.

### Samples, Their Global Reach, and Outline Methods

Paired river water, suspended sediment, and bed or bank sediment were collected from several of the world's largest rivers and their tributaries between 2013 and 2019, including the Murray and Darling in Australia, the Hong He (Red River), Irrawaddy, Salween, and Mekong in Southeast Asia, major tributaries of the Ganges (Karnali, Narayani, Koshi, Rapti, and Bagmati), and the Mackenzie and Yukon Rivers in North America. In addition, a number of small streams from Svalbard and the Alps were analyzed. The data are compared to the Amazon and the Ganges-Brahmaputra systems (10, 11). This sample collection is from a very wide range of catchments, with diverse lithological, climatic, geomorphological, and weathering characteristics. The Mackenzie is a shale-rich Arctic basin [where the majority of the clay is marine in origin (19)], whereas the Irrawaddy is a tropical basin, draining mixed sedimentary and magmatic terranes (20). The Himalayan tributaries of the Ganges are weathering limited, whereas the Murray–Darling system is transport limited. The Mackenzie is almost free from anthropogenic influence, whereas the Hong He and Mekong are extensively dammed (21).

Exchangeable ions on the suspended particulate matter (SPM) were determined either by reacting the sediment with calcite-saturated cobalt(III) hexammine chloride (CoHex; *SI Appendix*) (11) or by using ammonium chloride ( $\text{NH}_4\text{Cl}$ ).  $\text{NH}_4\text{Cl}$  is known to induce the dissolution of carbonate minerals if present (5), but, after filtering the data for exchange equilibrium (discussed below), the CEC and chemical compositions are within uncertainty for  $\text{NH}_4\text{Cl}$  and CoHex extractions (*SI Appendix*, Figs. S1–S3).

### Results

**Exchange Equilibrium between the Dissolved Load and Exchange Pool.** The measured exchange pool chemistry is in equilibrium with the river water chemistry, determined by comparing measurements of the exchange pool composition with modeled equilibrium values (*SI Appendix*). When  $\beta_{\text{Ca}}(\text{measured})$ , the fraction of Ca to other major cations in the exchange pool, deviated from the equilibrium value by more than the uncertainty of the CoHex data (*SI Appendix*, Fig. S2), samples were defined as not in equilibrium and excluded from calculations. The majority of these samples are  $\text{NH}_4\text{Cl}$  extractions of carbonate-rich samples, and the offset is consistent with carbonate dissolution. Strontium isotopes ( ${}^{87}\text{Sr}/{}^{86}\text{Sr}$ ) provide a robust tracer of the origin of the exchange pool (22). The very wide range in  ${}^{87}\text{Sr}/{}^{86}\text{Sr}$  in

the samples analyzed affords a unique opportunity to assess the chemical equilibrium between the exchange pool and coeval river water. There is a striking 1:1 relationship between  ${}^{87}\text{Sr}/{}^{86}\text{Sr}$  in the exchange pool of the SPM and  ${}^{87}\text{Sr}/{}^{86}\text{Sr}$  in the river water (Fig. 1), with a tighter relationship for the CoHex extractions ( $R^2 = 0.98$ ) compared to the  $\text{NH}_4\text{Cl}$  extractions ( $R^2 = 0.92$ ).  $\text{NH}_4\text{Cl}$  extractions which deviate significantly from the 1:1 line (Narayani and Trisuli Rivers in Nepal, the Peel in Canada, and the Salween) were offset because of small amounts of carbonate dissolution.

**Chemistry of the Riverine Exchange Pool.** The exchange pool chemistry is dominated by  $\text{Ca}^{2+}$  ( $\beta_{\text{Ca}}$ , the fraction of Ca in the exchange pool, is typically  $> 0.75$ , mean = 0.81). For the remaining major cations,  $\beta_{\text{Mg}} = 0.16$ ,  $\beta_{\text{Na}} = 0.017$ , and  $\beta_K = 0.018$  (Fig. 2A), on average. Although the river water and suspended sediment exchange pool are in equilibrium (based on equilibrium calculations and Sr isotopes), they are distinct because of exchange selectivity coefficients, such that  $\text{Ca}^{2+}$  and  $\text{Mg}^{2+}$  have stronger affinities for the exchange pool compared to  $\text{K}^+$  and  $\text{Na}^+$  (5). For example, the riverine exchange pool is enriched in  $\text{Ca}^{2+}$  and depleted in  $\text{Na}^+$ ,  $\text{K}^+$ , and  $\text{Mg}^{2+}$  relative to the river water (Fig. 2). This has been observed previously in both the Ganges-Brahmaputra and Amazon River basins as well as soil pore waters (10, 11, 23).

**Comparison with the Marine Exchange Pool.** There is a clear difference between the composition of the exchange pool for riverine sediments in equilibrium with river waters (present study), and marine sediments. Modern marine sediments have an exchange pool dominated by  $\text{Na}^+$  ( $\beta_{\text{Na}} = 0.6$ ; refs. 15 and 17). When rivers enter the oceans, the exchange pool of riverine particulate matter rapidly reacts with seawater, exchanging  $\text{Ca}^{2+}$  for  $\text{Na}^+$  (Eq. 1 and ref. 15). There are few measurements of unweathered

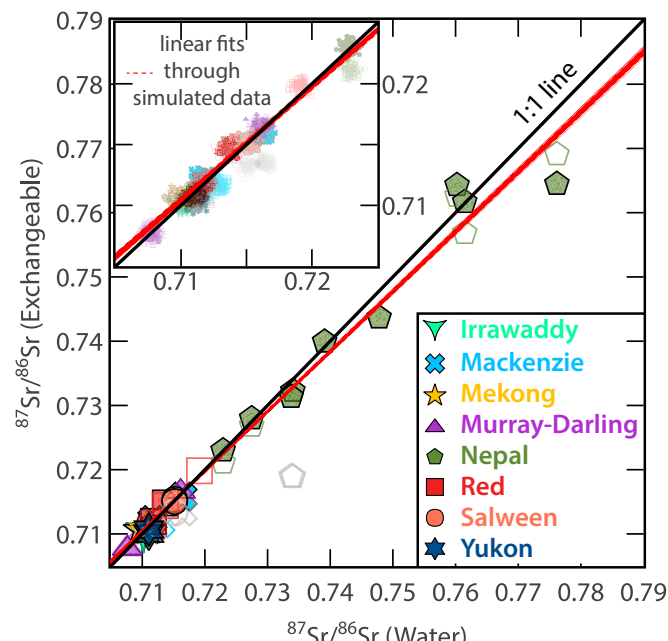


**Fig. 1.** Sr isotope ratio in the exchange pool as a function of Sr isotopes in the river water. Open and closed (black outline) symbols used the  $\text{NH}_4\text{Cl}$  and CoHex methods, respectively. Gray symbols indicate samples where the water and exchange pool are not in equilibrium. Uncertainties (500 parts per million [ppm]) synthetically distributed about the mean of the data are illustrated by the small points (Inset). Red lines are 100 examples of linear fits through this synthetic CoHex data.

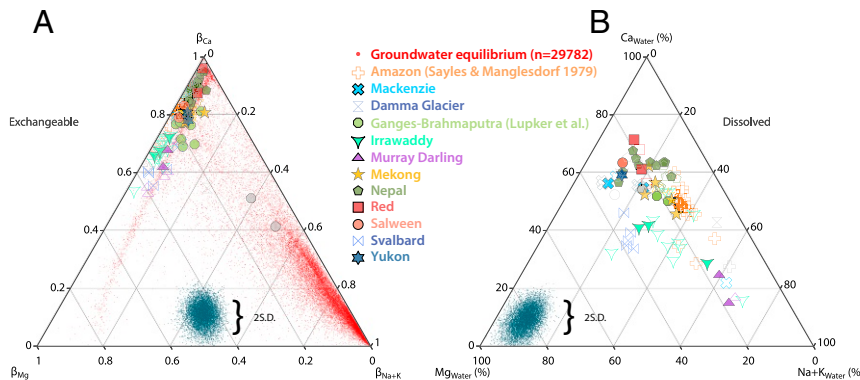


**Fig. 2.** Composition of the riverine exchange pool (*A*) and dissolved pool (*B*) as the percentage of the elements  $\text{Ca}^{2+}$ ,  $\text{Mg}^{2+}$ ,  $\text{K}^+$ , and  $\text{Na}^+$ . Amazon and Ganges-Brahmaputra data are from refs. 10 and 11, respectively. Open and closed (black outline) symbols used the  $\text{NH}_4\text{Cl}$  and CoHex methods, respectively. Gray symbols indicate samples where water and exchange pool are not in equilibrium. Small red points are exchange pool compositions calculated in equilibrium with groundwaters. Cluster of blue data points to indicate uncertainties are synthetic data distributed using the maximum uncertainties of the data determined using a Monte Carlo simulation.

(pristine) exhumed marine rocks. Some have  $\beta_{Na}$  in equilibrium with seawater (24–26), but some have lower  $\beta_{Na}$  of <0.18 (27, 28), suggesting a resetting by diagenetic or weathering processes. There are many more measurements of continental groundwaters, many of which are enriched in  $\text{Na}^+$ , likely linked to halite dissolution (nonsilicate  $\text{Na}^+$ ). We calculated the exchangeable cation compositions in equilibrium with such groundwaters from a compilation of almost 30,000 continental groundwaters (*SI Appendix*, Fig. 24, and ref. 29). The modal  $\beta_{Na}$  was 0.80 (mean of 0.56, interquartile range of 0.37 to 0.78; *SI Appendix*, Fig. S4), demonstrating that the unweathered continental exchange pool can retain a high  $\beta_{Na}$ .

**CEC.** The CEC of SPM was calculated as the sum of exchangeable  $\text{Ca}^{2+}$ ,  $\text{Mg}^{2+}$ ,  $\text{K}^+$ , and  $\text{Na}^+$  in milliequivalent units per 100 g (meq/100 g) of dry sediment, following convention. The range is comparable to that observed in other large river systems (<1 meq/100 g to 40 meq/100 g; *SI Appendix*, Fig. S5) (10, 11) and also in soils (23). This range is lower than the CEC estimates for clay minerals smectite (57 meq/100 g to 106 to meq/100 g) and kaolinite (17 meq/100 g to 35 to meq/100 g) (30), since fluvial SPM is always a mixture of multiple mineral phases. The sample from the Damma Glacier in the Swiss Alps, draining exclusively granite, has the lowest CEC, whereas the rivers with high CEC drain predominantly sedimentary terranes such as in the Mackenzie Basin (31).

The CEC correlates with the aluminum/silicon (Al/Si) ratio of the bulk sediment (11) (*SI Appendix*, Fig. S6;  $R^2 = 0.7$ , 0.8, and 0.7, for the Mekong, Sun Koshi, and Koshi River datasets, respectively). The Al/Si ratio is well documented to be a function of the grain size (32), which is strongly related to the proportion of clay mineral in the bulk sediment. Given that the fine fraction of rivers is dominated by clay minerals (33), this covariation provides a persuasive argument that the riverine CEC of SPM is dominated by clays. In weathering-limited systems, the majority of these clays are old marine sedimentary clays (19).

## Implications

**Increased Total Reactive Pool of Elements.** Although the CEC is conventionally quoted in units of meq/100 g, it is convenient to express the CEC of riverine SPM in microequivalents per liter of water ( $\mu\text{eq/L}$ ), taking into account the concentration of suspended sediment in the water column. Expressing CEC in these units allows direct comparison with the sum of the solute cations in the river water. The ratio of exchangeable Ca to solute Ca (Fig. 3) ranges from close to zero in some river systems to >0.5.

Half of our SPM samples carry more than ~5% of total Ca in the exchange pool, including major river systems such as the Salween, Mekong, Yukon, and rivers from Nepal.

Given that the exchange pool is in equilibrium with the river water, this implies that the total cationic load from chemical weathering (particularly of carbonates) has been underestimated at a global scale. The principal control on the ratio of exchangeable to dissolved cations is the concentration of sediment in the water column (Fig. 3). While the CEC varies by a factor of ~40, the SPM content varies by three orders of magnitude (from 0.01 g/L to 10 g/L) in our dataset, and, in extreme cases, such as glacial lake outburst floods, SPM concentrations can exceed 100 g/L (34). This is of particular importance to weathering fluxes, because regions of the world with high erosion rates (and thus

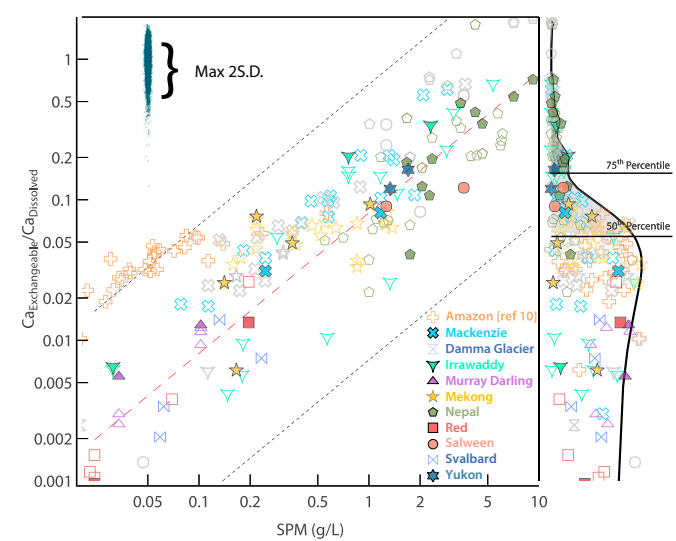


**Fig. 3.** Ratio of  $\text{Ca}^{2+}$  in the exchange pool relative to the dissolved pool (marginal plot shows frequency distribution showing 50th and 75th percentiles) versus the concentration of SPM in the river. Red dashed line is the best fit through the data. The black dotted lines bracket the data calculated using the 90th and 10th percentiles of  $\text{Ca}^{2+}$  in the exchange pool and the water to delineate upper and lower bounds. Open and closed (black outline) symbols used the  $\text{NH}_4\text{Cl}$  and CoHex methods, respectively. Gray symbols indicate water and exchange pool are not in equilibrium. Cluster of blue data points to indicate uncertainties are synthetic data distributed using the maximum uncertainties of the data determined using a Monte Carlo simulation.

typically elevated SPM contents) deliver the greatest weathering fluxes, consume the largest amounts of atmospheric carbon dioxide, and have the greatest sensitivity for climate feedbacks (35–37). It is these rivers from weathering-limited environments that have the greatest capacity for interaction between the river sediment and water, because they have the highest SPM contents. Several of the rivers here have a monsoonal hydrograph (Mekong, Irrawaddy, Salween, Nepal, Red) where SPM concentrations are highest during the monsoon (38), while solute concentrations are at their lowest (39). Therefore, maximum  $\text{Ca}_{\text{Exchange}}/\text{Ca}_{\text{Water}}$  coincides with the time of greatest solute flux. Transport-limited river basins with low SPM may also be significantly influenced by cation exchange processes in the soil environment, where the exchange pool may control the soil pore waters for many hundreds of years after the complete dissolution of primary mineral phases (22, 23). Cation exchange has long been proposed as a mechanism for buffering river water chemistry (7, 40), but a quantification of the component derived from ancient sedimentary rocks has proved elusive (9). The new data are used to quantify the supply of cations from the ancient marine exchange pool to modern weathering systems, as a function of the SPM content, the CEC, and chemical makeup of the lithogenic exchange pool. Below, we investigate the significance of the exchange pool for the silicate weathering fluxes.

**A Reduced Silicate Weathering Flux.** The substantial riverine exchange pool has important consequences for the calculation of silicate weathering fluxes, particularly where rivers erode large volumes of marine sedimentary rocks or continental rocks that have equilibrated with saline basement waters. In general, areas of greatest dissolved load flux are spatially correlated to easily eroded sedimentary rocks, and tectonically active regions contain uplifted sedimentary sequences characteristic of continental margins (41). Since the modern riverine exchange pool is dominated by  $\text{Ca}^{2+}$  (Fig. 2A), and marine sedimentary rocks have an exchange pool dominated by  $\text{Na}^+$ , the primary exchange reaction during uplift and exhumation is  $2\text{Na}_{\text{clay}}^+ \rightleftharpoons \text{Ca}_{\text{water}}^{2+}$ . The  $\text{Na}^+$ -dominated ancient marine exchange pool is released to river waters with an equivalent charge of  $\text{Ca}^{2+}$  removed from the river water (Eq. 1; the reverse of the reaction that occurs when riverine SPM is discharged into the sea). This is of importance, since most riverine estimates of modern silicate weathering fluxes are based on the assumption that, after  $\text{NaCl}$  salt correction, all remaining  $\text{Na}^+$  (denoted  $\text{Na}^*$ ) is derived exclusively from the dissolution of silicate minerals. Atmospheric  $\text{CO}_2$  is converted to bicarbonate in solution via silicate mineral dissolution in carbonic acid (42). In contrast, the release of  $\text{Na}^+$  from the exchange pool does not consume atmospheric  $\text{CO}_2$ . Since the silicate weathering flux and attendant  $\text{CO}_2$  consumption are calculated directly from the  $\text{Na}^*$  flux (42), any reduction in  $\text{Na}^*$  to account for ancient marine  $\text{Na}^+$  supplied via cation exchange ( $\text{Na}_{\text{ex}}^+$ ) is equivalent to the reduction in long-term carbon drawdown via silicate weathering. Denoting  $\text{Na}_{\text{sil}}$  as the silicate contribution of  $\text{Na}^+$ , corrected for both halite and cation exchange inputs, we quantified the percentage reduction in silicate weathering as

$$100 \cdot \frac{(\text{Na}^* - \text{Na}_{\text{sil}})}{\text{Na}^*} = \frac{100 \cdot \text{Na}_{\text{ex}}^+}{(\text{Na}_{\text{river}}^+ - \text{Cl}_{\text{river}}^-)}, \quad [2]$$

where a maximum estimate of  $\text{Na}_{\text{ex}}^+$  ( $\mu\text{eq}/\text{L}$ ) is given by the product of  $\beta_{\text{Na}}$  in equilibrium with seawater and the CEC (milliequivalents per kilogram) of the riverine SPM (grams per liter),

$$\text{Na}_{\text{ex}}^+ = \text{CEC} \cdot \text{SPM} \cdot \beta_{\text{Na}}. \quad [3]$$

Since some marine sediments are likely influenced by diagenesis lowering  $\beta_{\text{Na}}$ , in addition to some fraction of the riverine CEC resulting from neoformed clays in equilibrium with soil pore waters (19) (SI Appendix), we considered a generalized case where the reduction in the silicate weathering flux was parameterized as a function of  $\beta_{\text{Na}}$  between 0 and 0.6, the equilibrium value with seawater (SI Appendix, Fig. S7).

Since both  $\text{Na}^*$  and  $\text{CEC} \cdot \text{SPM}$  are determined for our sample set (Fig. 4, with the distributions indicated by the marginal plots), the reduction in the silicate weathering flux can be directly assessed as a function of  $\beta_{\text{Na}}$ . Assuming  $\beta_{\text{Na}} = 0.6$  (Fig. 4), the equilibrium value with seawater, many samples show a major reduction in  $\text{Na}^*$  (percentage reduction indicated by the contours) and thus the total silicate weathering flux. Some rivers plot above the 100% contour, indicating the entirety of riverine  $\text{Na}^*$  is derived from the exchange pool and that  $\beta_{\text{Na}}$  is  $<0.6$  in these catchments. For the Yukon, Irrawaddy, Salween, Mackenzie, Mekong, and Nepalese Rivers, the reduction in  $\text{Na}^*$  is greater than 25% (basin averages). In contrast, rivers such as the Amazon and the Murray–Darling, show less than a 10% reduction in  $\text{Na}^*$ . For  $\beta_{\text{Na}} = 0.6$ , the average reduction in  $\text{Na}^*$  is 53% (mean of the entire dataset). Assuming a more conservative  $\beta_{\text{Na}} = 0.2$  reduces  $\text{Na}^*$  by 32% once cation exchange is taken into account.

The contrasting behavior between different river basins reflects the interplay of the variables  $\text{Na}^*$ , CEC, and SPM. For example, although Nepalese rivers have among the lowest CEC (mean of 8.5 meq/100 g), they also have the lowest  $\text{Na}^*$  values (mean of 62  $\mu\text{mol}/\text{L}$ ) but highest suspended sediment concentrations (3.8 g/L). In contrast, the Amazon dataset (10) has similar  $\text{Na}^*$  (90  $\mu\text{mol}/\text{L}$ ), and much higher CEC (24 meq/100 g), but very low SPM (0.08 g/L). As noted above, high erosion basins

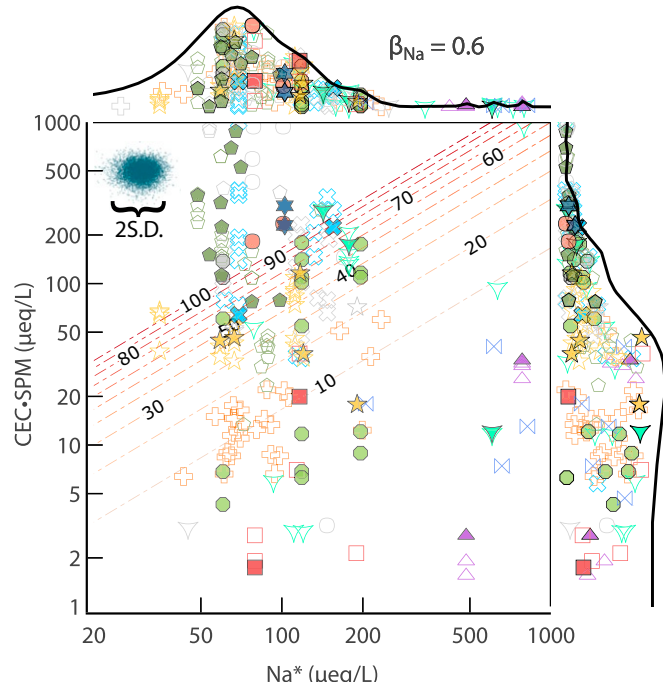


**Fig. 4.** CEC · SPM vs.  $\text{Na}^*$  contoured for the percentage reduction in silicate weathering flux  $100 \cdot (\text{Na}^* - \text{Na}_{\text{sil}})/\text{Na}^*$  ( $0 = \text{no change}$ ) calculated for  $\beta_{\text{Na}} = 0.6$ . Open and closed symbols used the  $\text{NH}_4\text{Cl}$  and CoHex methods, respectively. Gray symbols indicate water and exchange pool are not in equilibrium. Symbol legend is the same as for Fig. 2. Cluster of blue data points to indicate uncertainties are synthetic data distributed using the mean uncertainties of CEC · SPM and  $\text{Na}^*$  determined using a Monte Carlo simulation. SI Appendix, Fig. S8 shows contours calculated for  $\beta_{\text{Na}} = 0.2$ .

(weathering limited) are the most susceptible to a substantial influence from the exchange pool because of their high sediment load (Fig. 3). While weathering-limited basins are thought to be the most important for the silicate weathering feedback (36, 37, 43), they also have the largest reduction in  $\text{Na}^*$ , even for low  $\beta_{\text{Na}}$ .

**Extrapolation to Other Large Rivers.** To estimate CEC for river basins where data are not available, we exploited the linear dependency between CEC and the Al/Si of the SPM (*SI Appendix, Fig. S6*). Uncertainty was determined using the covariance matrix for Al/Si and CEC, which propagates the uncertainty of Al/Si to the CEC using a Monte Carlo simulation. For several of the world's largest rivers, we used published values of the Al/Si ratio (44–47) to determine the CEC and its associated uncertainty. Using  $\text{Na}^*$  and SPM concentration values (3), we determined the maximum percentage reduction in silicate weathering flux ( $100 \cdot (\text{Na}^* - \text{Na}_{\text{sil}})/\text{Na}^*$ ; Eq. 3 and Fig. 5).

The maximum discharge-weighted global average reduction in  $\text{Na}^*$  was determined as 28% ( $\beta_{\text{Na}} = 0.6$ ). A lower bound was estimated using  $\beta_{\text{Na}} = 0.2$  with a 12% reduction in  $\text{Na}^*$  (*SI Appendix, Fig. S9*). However, the global reduction in  $\text{Na}^*$  is uneven, with basins with high SPM load and/or low  $\text{Na}^*$  having the largest reductions in  $\text{Na}^*$ , at up to 100% for some of the world's largest rivers.

**Anthropogenic Influences.** It is worth noting that, in recent decades, many large river systems have suffered major reductions in their sediment loads because of hydropower dam construction (21). For example, the Red River samples are heavily affected by reduced SPM contents because of dams. Firstly, for rivers with a significant anthropogenic influence, such as the Red and the Mekong Rivers, the reduction in  $\text{Na}^*$  determined here underestimates the long-term reduction, because the suspended particulate load is lower than in its natural state. Secondly, the total flux of labile cations being delivered to the world's floodplains and oceans is being reduced by sediment trapping in dams because of the significant flux of elements carried in the exchange

pool. This is a temporary effect from a geological perspective, but it can skew estimates of chemical weathering downstream of major dams.

## Conclusions

We measured the chemistry and magnitude of the exchange pool in eight of the largest river systems on Earth. Strontium isotopes and comparison of the dissolved and exchange pool chemistry indicate chemical equilibrium between the dissolved and exchange pools. In some river systems, the flux of mobile elements in the exchange pool bonded weakly to mineral surfaces on SPM is comparable with that in the dissolved pool. This exchange pool delivers an important flux of base cations to the world's floodplains and oceans, currently in a state of perturbation by the rapid proliferation of dams. We demonstrate that, if at least part of the riverine exchange pool was marine in origin, this  $\text{Na}^+$ -rich marine exchange pool contributes to the modern river chemistry by exchanging with calcium. By comparing the exchange pool chemistry to that of the river water, we demonstrate that the global silicate weathering flux is 12 to 28% lower than previously thought, and up to 100% lower in some river systems. The reduction in the calculated silicate weathering flux is most marked in regions of the world with high erosion and high sediment loads, where chemical weathering reactions that control the negative climate feedback are most sensitive. This finding, that the magnitude of the silicate weathering flux needs to be reevaluated, adds to a series of recent studies (2, 48) that emphasize  $\text{CO}_2$  release during chemical weathering, and raise questions for the canonical view of the silicate weathering feedback.

## Materials and Methods

Materials and methods are summarized here; further details are provided in *SI Appendix*. Water and suspended sediment samples were mostly collected midchannel from boats, or, for smaller rivers, from bridges. Some recent bank deposits, from just above the water line, were collected and analyzed. Sediment was reacted with calcite-saturated CoHex (*SI Appendix*) (11), where the  $\text{Co}(\text{NH}_3)_6^{3+}$  ion displaces the exchangeable cations, but is buffered to calcite saturation, preventing the dissolution of calcite present

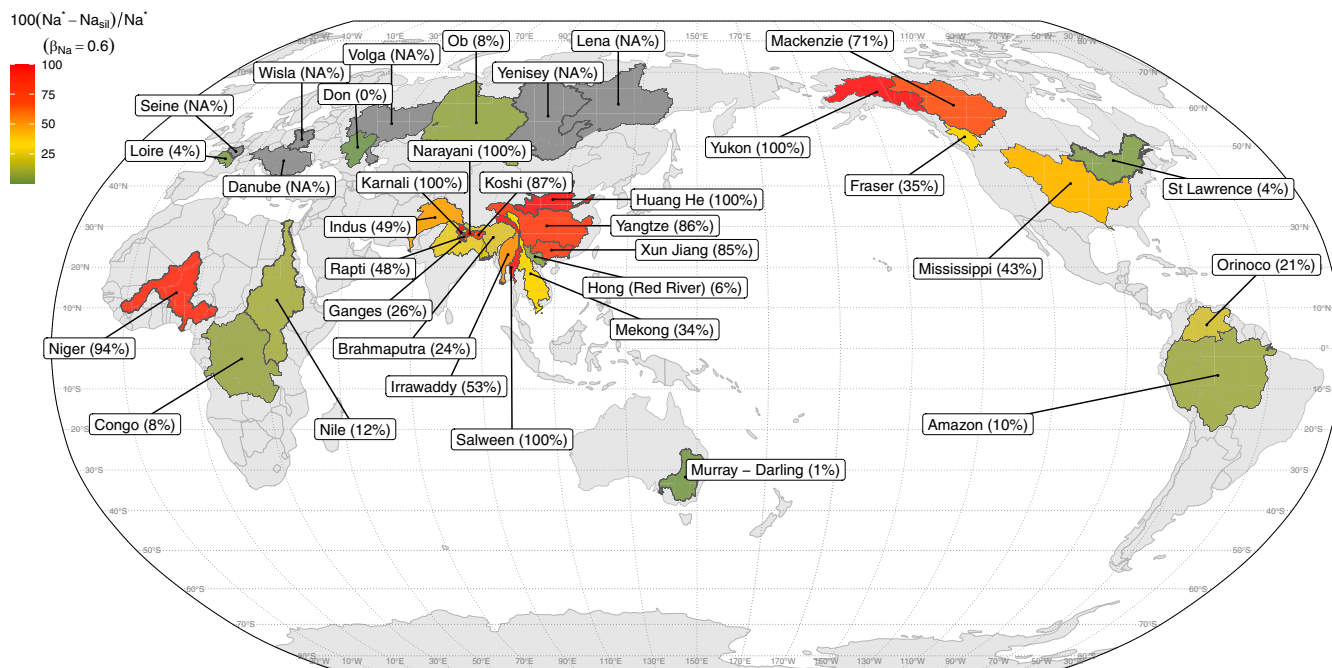


**Fig. 5.** Global map of large river basins colored for percentage reduction in the silicate weathering flux ( $100 \cdot (\text{Na}^* - \text{Na}_{\text{sil}})/\text{Na}^*$ ) calculated for  $\beta_{\text{Na}} = 0.6$  (*SI Appendix, Fig. S8* is equivalent calculated for  $\beta_{\text{Na}} = 0.2$ ). Basins in gray have chloride in excess of sodium ( $\text{Na}^* < 0$ ).

in some of the samples. Additional samples were reacted with ammonium chloride ( $\text{NH}_4\text{Cl}$ ) where the  $\text{NH}_4^+$  ion displaces exchangeable cations. Cation concentrations were determined by inductively coupled plasma optical emission spectroscopy or ion chromatography, and anions were determined by IC. The exchange pool extractions were measured either by ICP-OES or spectrometric ultraviolet absorbance, using matrix matched calibration lines. After filtering the data for exchange equilibrium, the CEC and chemical compositions are within uncertainty for  $\text{NH}_4\text{Cl}$  and CoHex extractions (SI Appendix, Figs S1–S3). Radiogenic strontium isotopic compositions were measured on a Neptune Plus multicollector–ICP–mass spectrometer (Thermo Scientific, University of Cambridge).

1. R. A. Berner, Z. Kothavala, Geocarb III: A revised model of atmospheric  $\text{CO}_2$  over phanerozoic time. *Am. J. Sci.* **301**, 182–204 (2001).
2. R. G. Hilton, A. J. West, Mountains, erosion and the carbon cycle. *Nat. Rev. Earth Environ.* **1**, 284–299 (2020).
3. J. Gaillardet, B. Dupré, P. Louvat, C. J. Allègre, Global silicate weathering and  $\text{CO}_2$  consumption rates deduced from the chemistry of large rivers. *Chem. Geol.* **159**, 3–30 (1999).
4. G. Sposito *et al.*, Surface geochemistry of the clay minerals. *Proc. Natl. Acad. Sci. U.S.A.* **96**, 3358–3364 (1999).
5. C. A. J. Appelo, Multicomponent ion exchange and chromatography in natural systems. *Rev. Mineral. Geochem.* **34**, 193–227 (1996).
6. J. A. Andrews, W. H. Schlesinger, Soil  $\text{CO}_2$  dynamics, acidification, and chemical weathering in a temperate forest with experimental  $\text{CO}_2$  enrichment. *Global Biogeochem. Cycles* **15**, 149–162 (2001).
7. D. W. Clow, M. A. Mast, Mechanisms for chemostatic behavior in catchments: Implications for  $\text{CO}_2$  consumption by mineral weathering. *Chem. Geol.* **269**, 40–51 (2010).
8. J. S. Scheingross *et al.*, Preservation of organic carbon during active fluvial transport and particle abrasion. *Geology* **47**, 958–962 (2019).
9. T. E. Cerling, B. L. Pederson, K. L. Von Damm, Sodium-calcium ion exchange in the weathering of shales: Implications for global weathering budgets. *Geology* **17**, 552–554 (1989).
10. F. L. Sayles, P. C. Mangelsdorf Jr, Cation-exchange characteristics of Amazon River suspended sediment and its reaction with seawater. *Geochem. Cosmochim. Acta* **43**, 767–779 (1979).
11. M. Lupker, C. France-Lanord, B. Lartiges, Impact of sediment-seawater cation exchange on Himalayan chemical weathering fluxes. *Earth Surf. Dyn.* **4**, 675–684 (2016).
12. G. E. Likens, C. T. Driscoll, D. C. Buso, Long-term effects of acid rain: Response and recovery of a forest ecosystem. *Science* **272**, 244–246 (1996).
13. R. S. Hindshaw, S. M. Aceiro, A. M. Piotrowski, E. T. Tipper, Decoupling of dissolved and bedrock neodymium isotopes during sedimentary cycling. *Geochem. Pers. Lett.* **8**, 43–46 (2018).
14. S. Samanta, T. K. Dalai, Dissolved and particulate Barium in the Ganga (Hooghly) River estuary, India: Solute-particle interactions and the enhanced dissolved flux to the oceans. *Geochem. Cosmochim. Acta* **195**, 1–28 (2016).
15. F. L. Sayles, P. C. Mangelsdorf Jr, The equilibration of clay minerals with sea water: Exchange reactions. *Geochem. Cosmochim. Acta* **41**, 951–960 (1977).
16. P. Michalopoulos, R. C. Aller, Rapid clay mineral formation in Amazon delta sediments: Reverse weathering and oceanic elemental cycles. *Science* **270**, 614–617 (1995).
17. P. Y. Henry, "Relationship between porosity, electrical conductivity, and cation exchange capacity in Barbados Wedge sediments" in *Proceedings of the Ocean Drilling Program, Scientific Results*, T. H. Shipley *et al.*, Eds. (Texas A&M University, 1997), vol. 156, pp. 137–149.
18. R. A. Berner *et al.*, Comment and reply on "Sodium-calcium ion exchange in the weathering of shales: Implications for global weathering budgets". *Geology* **18**, 190–191 (1990).
19. M. Dellinger *et al.*, Lithium isotopes in large rivers reveal the cannibalistic nature of modern continental weathering and erosion. *Earth Planet Sci. Lett.* **401**, 359–372 (2014).
20. E. Garzanti, J. G. Wang, G. Vezzoli, M. Limonta, Tracing provenance and sediment fluxes in the Irrawaddy River basin (Myanmar). *Chem. Geol.* **440**, 73–90 (2016).
21. X. Li, J. P. Liu, Y. Saito, V. L. Nguyen, Recent evolution of the Mekong Delta and the impacts of dams. *Earth Sci. Rev.* **175**, 1–17 (2017).
22. T. Bullen, A. White, A. Blum, J. Harden, M. Schulz, Chemical weathering of a soil chronosequence on granitoid alluvium: II. Mineralogic and isotopic constraints on the behavior of strontium. *Geochem. Cosmochim. Acta* **61**, 291–306 (1997).
23. A. F. White *et al.*, Chemical weathering of a marine terrace chronosequence, Santa Cruz, California II: Solute profiles, gradients and linear approximations of contemporary and long-term weathering rates. *Geochem. Cosmochim. Acta* **72**, 36–68 (2009).
24. K. L. Von Damm, "Geochemistry of shale groundwaters: Survey of available data and postulated mineralogic controls on composition" (Tech. Rep. ORNL/TM-10488, US Department of Energy, 1987).
25. S. Zhang, J. J. Sheng, Z. Qiu, Maintaining shale stability using polyether amine while preventing polyether amine intercalation. *Appl. Clay Sci.* **132–133**, 635–640 (2016).
26. A. M. Fernández *et al.*, Applying the squeezing technique to highly consolidated clay-rocks for pore water characterisation: Lessons learned from experiments at the Mont Terri rock laboratory. *Appl. Geochem.* **49**, 2–21 (2014).
27. E. Gaucher *et al.*, ANDRA underground research laboratory: Interpretation of the mineralogical and geochemical data acquired in the Callovian-Oxfordian formation by investigative drilling. *Phys. Chem. Earth* **29**, 55–77 (2004).
28. L. Jin *et al.*, Mineral weathering and elemental transport during hillslope evolution at the Susquehanna/Shale Hills Critical Zone Observatory. *Geochem. Cosmochim. Acta* **74**, 3669–3691 (2010).
29. M. Blondes *et al.*, U.S. Geological Survey National Produced Waters Geochemical Database v2.3. <https://doi.org/10.5066/F7J964W8>. Accessed 11 December 2020.
30. C. Ma, R. A. Eggleton, Cation exchange capacity of kaolinite. *Clay Clay Miner.* **47**, 174–180 (1999).
31. R. Millot, J. Gaillardet, B. Dupré, C. J. Allègre, Northern latitude chemical weathering rates: Clues from the Mackenzie river basin, Canada. *Geochem. Cosmochim. Acta* **67**, 1305–1329 (2003).
32. J. Bouchez, J. Gaillardet, C. France-Lanord, L. Maurice, P. Dutra-Maia, Grain size control of river suspended sediment geochemistry: Clues from Amazon River depth profiles. *Geochem. Geophys. Geosyst.* **12**, 12 (2011).
33. J. L. Guyot *et al.*, Clay mineral composition of river sediments in the Amazon Basin. *Catena* **71**, 340–356 (2007).
34. K. L. Cook, C. Andermann, F. Gimbert, B. R. Adhikari, N. Hovius, Glacial lake outbursts floods as drivers of fluvial erosion in the Himalaya. *Science* **362**, 53–57 (2018).
35. A. J. West, A. Galy, M. Bickle, Tectonic and climatic controls on silicate weathering. *Earth Planet Sci. Lett.* **235**, 211–228 (2005).
36. I. J. Larsen, D. R. Montgomery, H. M. Greenberg, The contribution of mountains to global denudation. *Geology* **42**, 527–530 (2014).
37. K. Maher, C. P. Chamberlain, Hydrologic regulation of chemical weathering and the geologic carbon cycle. *Science* **343**, 1502–1504 (2014).
38. C. Andermann, A. Crave, R. Gloaguen, P. Davy, S. Bonnet, Connecting source and transport: Suspended sediments in the Nepal Himalayas. *Earth Planet. Sci. Lett.* **351–352**, 158–170 (2012).
39. E. T. Tipper *et al.*, The short term climatic sensitivity of carbonate and silicate weathering fluxes: Insight from seasonal variations in river chemistry. *Geochem. Cosmochim. Acta* **70**, 2737–2754 (2006).
40. R. A. Berner, J. L. Rao, S. Chang, R. O'Brien, C. K. Keller, Seasonal variability of adsorption and exchange equilibria in soil waters. *Aquat. Geochem.* **4**, 273–290 (1998).
41. M. E. Raymo, W. F. Ruddiman, P. N. Froelich, Influence of late Cenozoic mountain building on ocean geochemical cycles. *Geology* **16**, 649–653 (1988).
42. A. Galy, C. France-Lanord, Weathering processes in the Ganges-Brahmaputra basin and the riverine alkalinity budget. *Chem. Geol.* **159**, 31–60 (1999).
43. A. J. West, Thickness of the chemical weathering zone and implications for erosional and climatic drivers of weathering and for carbon-cycle feedbacks. *Geology* **40**, 811–814 (2012).
44. G. Bayon *et al.*, Rare earth elements and neodymium isotopes in world river sediments revisited. *Geochem. Cosmochim. Acta* **170**, 17–38 (2015).
45. J. Gaillardet, B. Dupré, C. J. Allègre, Geochemistry of large river suspended sediments: Silicate weathering or recycling tracer? *Geochem. Cosmochim. Acta* **63**, 4037–4051 (1999).
46. T. Ahmad, P. P. Khanna, G. J. Chakrapani, S. Balakrishnan, Geochemical characteristics of water and sediment of the Indus River, Trans-Himalaya, India: Constraints on weathering and erosion. *J. Asian Earth Sci.* **16**, 333–346 (1998).
47. V. V. Gordeev, B. Beeskow, V. Rachold, "Geochemistry of the Ob and Yenisey estuaries: A comparative study" (Tech. Rep. 557, Alfred Wegener Institute, 2007).
48. M. A. Torres, A. J. West, G. Li, Sulphide oxidation and carbonate dissolution as a source of  $\text{CO}_2$  over geological timescales. *Nature* **507**, 346–349 (2014).

**Data Availability.** All study data are included in the article and *SI Appendix*.

**ACKNOWLEDGMENTS.** This work was funded by National Environmental Research Council Grants NE/K000705/1, NE/M001865/1, NE/N007441/1, and NE/P011659/1 to E.T.T., and NERC Arctic Bursary Award & European Research Council Starting Grant ROC-CO2 678779 to R.G.H. Mackenzie River samples were collected under research licenses 15288 and 16106. Many people assisted in the collection of samples in the field. C. Parish built our field equipment. H. Chapman conducted some of the Sr isotope chemistry. S. Souanef-Ureta conducted some of the  $\text{NH}_4\text{Cl}$  extractions. M.-L. Bagard ensured the flawless running of the Cambridge Plasma Labs. The manuscript was improved by two thoughtful anonymous reviewers.